Chinese Journal of Natural Medicines

The transcriptomic-based disease network reveals synergistic therapeutic effect of total alkaloids from *Coptis chinensis* and total ginsenosides from *Panax ginseng* on type 2 diabetes mellitus

Qian Chen, Shuying Zhang, Xuanxi Jiang, Jie Liao, Xin Shao, Xin Peng, Zheng Wang, Xiaoyan Lu, Xiaohui Fan

Citation: Qian Chen, Shuying Zhang, Xuanxi Jiang, Jie Liao, Xin Shao, Xin Peng, Zheng Wang, Xiaoyan Lu, Xiaohui Fan, The transcriptomic-based disease network reveals synergistic therapeutic effect of total alkaloids from *Coptis chinensis* and total ginsenosides from *Panax ginseng* on type 2 diabetes mellitus, Chinese Journal of Natural Medicines, 2025, 23(8), 997-1008. doi: 10.1016/S1875-5364(25)60935-6.

View online: https://doi.org/10.1016/S1875-5364(25)60935-6

Chinese Journal of Natural Medicines 23 (2025) 997-1008

Contents lists available at ScienceDirect

Chinese Journal of Natural Medicines

journal homepage: www.cjnmcpu.com/

Original article

The transcriptomic-based disease network reveals synergistic therapeutic effect of total alkaloids from *Coptis chinensis* and total ginsenosides from *Panax ginseng* on type 2 diabetes mellitus

Qian Chen[a,b,Δ], Shuying Zhang[a,c,Δ], Xuanxi Jiang[a], Jie Liao[a,b], Xin Shao[a,b], Xin Peng[d], Zheng Wang[a,b], Xiaoyan Lu[a,*], Xiaohui Fan[a,b,*]

[a] *Pharmaceutical Informatics Institute, College of Pharmaceutical Sciences, Zhejiang University, Hangzhou 310058, China*
[b] *National Key Laboratory of Chinese Medicine Modernization, Innovation Center of Yangtze River Delta, Zhejiang University, Jiaxing 314100, China*
[c] *School of Clinical Medicine, Shanghai University of Medicine & Health Sciences, Shanghai 201318, China*
[d] *Ningbo Municipal Hospital of TCM, Affiliated Hospital of Zhejiang Chinese Medical University, Ningbo 315100, China*

ARTICLE INFO

Article history:
Received 11 October 2024
Revised 8 January 2025
Accepted 23 February 2025
Available online 20 August 2025

Keywords:
Total alkaloids from *Coptis chinensis*
Alkaloids
Total ginsenosides from *Panax ginseng*
Component compatibility
Network pharmacology
Type 2 diabetes mellitus

ABSTRACT

Coptis chinensis Franch. and *Panax ginseng* C. A. Mey. are traditional herbal medicines with millennia of documented use and broad therapeutic applications, including anti-diabetic properties. However, the synergistic effect of total alkaloids from *Coptis chinensis* and total ginsenosides from *Panax ginseng* on type 2 diabetes mellitus (T2DM) and its underlying mechanism remain unclear. The research demonstrated that the optimal ratio of total alkaloids from *Coptis chinensis* and total ginsenosides from *Panax ginseng* was 4∶1, exhibiting maximal efficacy in improving insulin resistance and gluconeogenesis in primary mouse hepatocytes. This combination demonstrated significant synergistic effects in improving glucose tolerance, reducing fasting blood glucose (FBG), the weight ratio of epididymal white adipose tissue (eWAT), and the homeostasis model assessment of insulin resistance (HOMA-IR) in leptin receptor-deficient (db/db) mice. Subsequently, a T2DM liver-specific network was constructed based on RNA sequencing (RNA-seq) experiments and public databases by integrating transcriptional properties of disease-associated proteins and protein-protein interactions (PPIs). The network recovery index (NRI) score of the combined treatment group with a 4∶1 ratio exceeded that of groups treated with individual components. The research identified that activated adenosine 5'-monophosphate-activated protein kinase (AMPK)/acetyl-CoA carboxylase (ACC) signaling in the liver played a crucial role in the synergistic treatment of T2DM, as verified by western blot experiment in db/db mice. These findings demonstrate that the 4∶1 combination of total alkaloids from *Coptis chinensis* and total ginsenosides from *Panax ginseng* significantly improves insulin resistance and glucose and lipid metabolism disorders in db/db mice, surpassing the efficacy of individual treatments. The synergistic mechanism correlates with enhanced AMPK/ACC signaling pathway activity.

1. Introduction

Diabetes mellitus represents a chronic metabolic disorder with multifaceted pathogenesis, demonstrating increasing prevalence globally, with type 2 diabetes mellitus (T2DM) constituting over 90% of cases [1, 2]. China bears a significant diabetes burden, with prevalence rates increasing from 10.9% in 2013 to 12.4% in 2018 [3]. As a major global health crisis, diabetes mellitus leads to chronic progressive deterioration of multiple tissues and organs, reducing life expectancy by 4–10 years and elevating mortality risks from cardiovascular disease, kidney disease, and cancer [4]. Despite numerous approved treatments for T2DM, approximately 11.3% of global mortality remains diabetes-related [5]. International Diabetes Federation statistics indicate that 6.7 million individuals succumbed to diabetes and its complications in 2021 alone. Contemporary research demonstrates that combination therapy exhibits superior overall efficacy compared to monotherapy, typically requiring lower dosages, thereby enhancing safety and tolerability [6, 7]. Consequently, the exploration of effective combination treatment protocols remains a critical and challenging objective in T2DM research.

Traditional Chinese medicine (TCM) has served a crucial role in treating diabetes (known as "Xiaoke" in TCM) throughout the millennia. *Coptis chinensis* and *Panax ginseng*, initially documented in the *Shen Nong Ben Cao Jing* (*Shennong's Classic on Materia Medica*, 100–200 AD) and classified as top-grade medicines, represent two renowned Chinese medicinal materials for diabetes treatment [8]. *Coptis chinensis* and *Panax ginseng* were frequently incorporated into TCM formulations for diabetes treatment [9]. Contemporary research confirms their effectiveness in treating diabetes, demonstrating their capacity to reduce blood glucose, insulin secretion, and insulin resistance in T2DM pa-

* Corresponding author.
E-mail addresses: Luxy@zju.edu.cn (X. Lu); fanxh@zju.edu.cn (X. Fan)
Δ These authors contributed equally to this work.

https://doi.org/10.1016/S1875-5364(25)60935-6

tients. Studies indicate that *Coptis chinensis* protects β cell function in diabetic mice through oxidative stress reduction and β cell damage prevention [10]. The total alkaloids from *Coptis chinensis* ameliorate glucose and lipid metabolism disorders, enhance insulin signal transduction in T2DM rat brains, and improve cognitive dysfunction [11]. Berberine, the principal active component in *Coptis chinensis*, exhibits hypoglycaemic and hypolipidaemic effects through multiple pathways. It enhances insulin receptor expression and inhibits deoxycholic acid biotransformation by *Ruminococcus bromii*, thereby reducing blood glucose in T2DM patients [12, 13]. In mice maintained on a high-fat and high-sucrose diet, berberine mediates liver autophagy and activates fibroblast growth factor 21 through a sirtuin 1 (SIRT1)-dependent mechanism to reduce hepatic steatosis and maintain whole-body energy metabolism [14]. Berberine also targets the potassium voltage-gated channel, subfamily H (eag-related), member 6 (KCNH6) to enhance insulin secretion [15]. Ginsenosides, the primary bioactive constituents in *Panax ginseng*, significantly improve hyperglycemia and dyslipidemia in diabetic rats by stimulating glucagon-like peptide-1 (GLP1) secretion and up-regulating proglucagon gene expression [16]. Research shows that ginsenoside Rg1 inhibits hepatic gluconeogenesis by activating protein kinase B (AKT) and promoting AKT-forkhead box O1 (FOXO1) interaction [17]. Ginsenoside Rb1 effectively prevents metabolic disorders and insulin resistance in T2DM mice, correlating with intestinal microbiota remodeling and related metabolite alterations [18].

The synergistic effect of *Coptis chinensis* and *Panax ginseng* in T2DM treatment and its underlying mechanisms remain incompletely understood. The liver, a major insulin-sensitive organ, plays a crucial role in T2DM pathological mechanisms and treatment approaches [19, 20]. Total alkaloids and total ginsenosides constitute the primary active components of *Coptis chinensis* Franch. and *Panax ginseng* C. A. Mey., respectively. This study initially evaluated the improvement effects of various compatibility ratios of total alkaloids from *Coptis chinensis* and total ginsenosides from *Panax ginseng* on insulin resistance and gluconeogenesis in primary mouse hepatocytes, examining glucose metabolism, lipid accumulation, oxidative stress, and mitochondrial function to determine the optimal compatibility ratio. Subsequently, leptin receptor-deficient (db/db) mice were utilized to compare the therapeutic effects of total alkaloids from *Coptis chinensis* and total ginsenosides from *Panax ginseng*, administered individually and in combination, on T2DM improvement, considering body weight, organ coefficients, glucose metabolism, insulin resistance, and lipid metabolism. Furthermore, based on RNA sequencing (RNA-seq) experiments and public databases, a T2DM liver-specific network was constructed by integrating transcriptional properties of disease-associated proteins and protein-protein interactions (PPIs). Finally, network topology and transcriptomics-based approach (NTRA) and network recovery index (NRI), network analysis methods previously proposed, were employed to compare and evaluate the holistic recovery effects of drugs on T2DM liver-specific network, and to analyze their potential synergistic mechanisms in conjunction with molecular docking.

2. Materials and methods

2.1. Animals and reagents

Male C57BL/6 mice (6–8 weeks, 24–26 g) were obtained from Zhejiang Vital River Laboratory Animal Technology Co., Ltd. (Jiaxing, China). Male db/db mice and db/m mice aged 6–8 weeks were acquired from Gempharmatech Co., Ltd. (Changzhou, China). All mice were maintained in an individual ventilated cage system under controlled conditions of 50% ± 10% humidity and 25 ± 1 °C temperature, with a 12-h light/12-h dark cycle and unrestricted access to food and water. All animal experiments were conducted in accordance with the Guidelines of the Animal Care and Use Committee of Zhejiang University School of Medicine (ZJU20240067).

Total ginsenosides from *Panax ginseng* (1.53% extraction yield and 97.93% purity) and total alkaloids from *Coptis chinensis* (8.53% extraction yield and 97.90% purity) were extracted by Shanghai Winherb Medical Science Co., Ltd. (Shanghai, China) from *Panax ginseng* (22012001) and *Coptis chinensis* (21112901) obtained from Taizhou Baicao Chinese Medicine Drinks Slice Co., Ltd. (Taizhou, China). The extraction methodology and total ion chromatogram are presented in Supplemental material (Figs. S1 and S2). Sodium pyruvate and sodium lactate were supplied by Aladdin Biochemical Technology Co., Ltd. (Shanghai, China). Glucagon was obtained from MedChemExpress (Monmouth Junction, NJ, USA). Palmitic acid (PA) and oleic acid (OA) were procured from Sigma-Aldrich (St. Louis, MO, USA). Mouse insulin ELISA (80-INSMS-E01) was acquired from ALPCO (Elk Grove, CA, USA). The assay kits for total cholesterol (TC, A111-1-1), triglyceride (TG, A110-1-1), high-density lipoprotein cholesterol (HDL-C, A112-1-1), and low-density lipoprotein cholesterol (LDL-C, A113-1-1) were obtained from Nanjing Jiancheng Bioengineering Institute (Nanjing, China).

2.2. Isolation and culture of primary mouse hepatocytes

Primary mouse hepatocytes were isolated from 6- to 8-week-old male C57BL/6 mice through two-step collagenase liver perfusion. The liver was perfused *in situ* with prewarmed (37 °C) buffer solution I (0.95 g·L^{-1} EGTA, 8.3 g·L^{-1} NaCl, 0.5 g·L^{-1} KCl, 2.388 g·L^{-1} HEPES) and buffer solution II (3.9 g·L^{-1} NaCl, 0.5 g·L^{-1} KCl, 2.388 g·L^{-1} HEPES, 0.532 g·L^{-1} $CaCl_2$, 0.5 g·L^{-1} collagenase IV, and 4.17 g·L^{-1} bovine serum albumin (BSA)) until complete liver swelling occurred. The digested liver cells were filtered through a 70-μm cell strainer and centrifuged at 800 r·min^{-1} for 4 min at 4 °C. Cell precipitation was suspended in 45% Percoll solution and centrifuged at 1300 r·min^{-1} for 4 min at 4 °C. The cell pellet was resuspended in Dulbecco's modified Eagle's medium (DMEM) containing 10% (*V*/*V*) fetal bovine serum (FBS) (Gibco, CA, USA), 100 units·mL^{-1} penicillin, and 100 μg·mL^{-1} streptomycin. The primary mouse hepatocytes were plated in 96-well (4 × 10^4 cells/well), 12-well (5 × 10^5 cells/well), and 6-well (1 × 10^6 cells/well) plates, and maintained in a humidified atmosphere with 5% CO_2 at 37 °C.

2.3. Cell viability assay

The culture medium was replaced with fresh DMEM supplemented with total alkaloids from *Coptis chinensis* and total ginsenosides from *Panax ginseng*. The blank control group contained only DMEM without primary hepatocytes. Following 24-h incubation, 10 μL of Cell Counting Kit-8 (CCK8) reagent was added to each well, and the plates were incubated for an additional 2 h. The optical density (OD) values of solutions were measured at 450 nm using an Infinite M1000 Pro microplate reader (TECAN, Switzerland). Cell viability was calculated as the OD of the treatment group normalized to the control group after subtracting the OD value of the blank control group.

2.4. Hepatic glucose output

After culturing in low-glucose DMEM for 12 h, primary mouse hepatocytes were washed three times with PBS solution and starved for another 3 h. Subsequently, the medium was replaced with fresh medium (2 mmol·L^{-1} sodium pyruvate, 20 mmol·L^{-1} sodium lactate, and 100 nmol·L^{-1} glucagon dissolved in glucose-free DMEM without phenol red) and incubated for 6 h.

The control group was maintained without glucagon, while the treatment group received varying proportions of total alkaloids from *Coptis chinensis* and total ginsenosides from *Panax ginseng*. Glucose concentration in the culture supernatant was determined using the glucose oxidase-peroxidase assay kit (361510, Shanghai Rongsheng Biotech Co., Ltd., Shanghai, China) following the manufacturer's protocol.

2.5. Hepatic insulin resistance experiment

The primary mouse hepatocytes were washed three times with PBS solution and treated with DMEM containing 5 mmol·L^{-1} PA and 10 mmol·L^{-1} OA for 12 h. The treatment group received varying proportions of total alkaloids from *Coptis chinensis* and total ginsenosides from *Panax ginseng*, while the model group received an equivalent concentration of BSA. Following drug intervention, lipid accumulation, oxidative stress, and mitochondrial damage in primary hepatocytes were assessed using Oil Red O staining (Oil Red O stain kit, G1262, Solarbio, Beijing, China), Reactive Oxygen Species Assay Kit (S0033, Beyotime Institute of Biotechnology, Jiangsu, China) and CellTiter-Glo® Luminescent Cell Viability Assay (G7570, Promega, Madison, WI, USA) according to the manufacturer's specifications.

2.6. Animal experiments

Based on body weight and fasting blood glucose (FBG) levels, db/db mice were randomly divided into five groups: model group (n = 12), total alkaloids from *Coptis chinensis* (HL) group (n = 6), total ginsenosides from *Panax ginseng* (RS) group (n = 6), the combination of total alkaloids from *Coptis chinensis* and total ginsenosides from *Panax ginseng* (HLRS) group (n = 12) and metformin (Met) group (n = 6). The db/m mice (n = 12) served as the control group. The preceding *in vitro* experiments demonstrated an optimal ratio of 4∶1 for total alkaloids from *Coptis chinensis* to total ginsenosides from *Panax ginseng*. Considering clinical dosages and preliminary experimental results *in vivo*, the daily dosages were established at 3.28 g raw medicinal herbs/kg and 0.82 g raw medicinal herbs·kg^{-1}, respectively, based on human-to-mouse dosage conversions [21]. The mice in HL group, RS group, HLRS group and Met group received intragastric administration of total alkaloids from *Coptis chinensis* (3.28 g raw medicinal herbs·kg^{-1}·d^{-1}), total ginsenosides from *Panax ginseng* (0.82 g raw medicinal herbs·kg^{-1}·d^{-1}), their combination, and metformin (200 mg·kg^{-1}·d^{-1}), respectively. Body weight was recorded weekly. FBG was measured before treatment and at 8 weeks post-treatment. After 8 weeks of administration, all rats were anesthetized and sacrificed, and liver tissue, blood, epididymal white adipose tissue (eWAT), inguinal white adipose tissue (iWAT), and perirenal white adipose tissue (pWAT) were collected. The organ coefficient (%) was calculated as: organ coefficient = organ mass (g)/body weight (g) × 100% [18].

2.7. Biochemical analysis

All mice underwent glucose tolerance test (GTT) *via* intraperitoneal injection of 1 g·kg^{-1} glucose after 16 h of fasting, or insulin tolerance test (ITT) *via* intraperitoneal injection of 0.75 U·kg^{-1} insulin after 6 h of fasting. Blood glucose levels were monitored through the tail vein at 0, 15, 30, 60, and 120 min. The area under the curve (AUC) was calculated based on the blood glucose values at each time point. Serum levels of TC, TG, HDL-C, LDL-C, and fasting serum insulin (FINS) were detected according to the manufacturers' instructions. The homeostasis model assessment of insulin resistance (HOMA-IR) was calculated using the following formula: HOMA-IR = [FBG (mmol·L^{-1}) × 18 × FINS (ng·mL^{-1}) × 24]/405 [22].

2.8. Histopathological study

The liver tissues of mice were fixed in 10% formalin for 24 h and subsequently embedded in paraffin or rapidly frozen in liquid nitrogen before transfer to storage at −80 °C. Liver sections were cut and mounted on slides for histopathological analysis using hematoxylin and eosin (H&E), periodic acid-schiff (PAS), or oil red O staining.

2.9. RNA-seq experiment

Liver tissues were harvested from the mice and immediately snap-frozen in liquid nitrogen, then stored at −80 °C until further processing. Total RNA was extracted using the TRIzol reagent (Invitrogen, USA), and RNA integrity and purity were assessed *via* agarose gel electrophoresis and the Agilent 2100 Bioanalyzer system (Agilent Technologies, USA). Sequencing libraries were prepared from 1 μg of total RNA per sample using the NEBNext® UltraTM RNA Library Prep Kit for Illumina® (New England Biolabs, USA), following the manufacturer's protocol. After purification, cDNA fragments approximately 250–300 bp in length were selected and enriched *via* polymerase chain reaction (PCR) amplification. The resulting PCR products were purified, and library quality was evaluated using the Agilent 2100 Bioanalyzer. High-throughput RNA sequencing was conducted by Novogene Co., Ltd. (Beijing, China) on the Illumina NovaSeq 6000 platform.

2.10. T2DM liver-specific network construction

T2DM-related genes were retrieved from the GeneCards database (https://www.genecards.org/) using a "Relevance score" > 30. Liver-expressed genes were then obtained from the Human Protein Atlas (HPA, https://www.proteinatlas.org/) by selecting entries with "Evidence at protein level" under the "HPA.evidence" criterion. These two datasets were intersected with differentially expressed genes identified through RNA-seq analysis to yield 810 high-confidence, liver-specific T2DM-associated targets. PPI data were obtained from the STRING database (https://cn.string-db.org/), and interactions with a combined confidence score greater than 0.7, supported by "experimental" and "co-occurrence" evidence channels, were retained. The resulting PPI network was visualized using Cytoscape (v3.82). Network topological properties, including degree and betweenness centrality of each node, were calculated using NetworkAnalyzer plugin in Cytoscape.

2.11. NRI for T2DM liver-specific network

The NRI is a network-based evaluation algorithm designed to assess the capacity of therapeutic interventions to restore homeostasis within disease-specific biological networks [23]. To simulate disease-associated network imbalance, gene expression changes within the T2DM-related liver network were compared between normal and diabetic conditions. The extent of recovery following drug intervention was then evaluated by measuring the overall reversion of gene expression levels toward the normal state. NRI was calculated as the sum of RRODN values for all genes (equation 1), including both up-regulated and down-regulated genes, as defined by an absolute value of [$\log_2$ (E_{normal}) − $\log_2$ ($E_{disease}$)] exceeding 0.5. RRODN, representing node recovery ability of individual nodes, was measured by considering topology and EoR-positive (EoR) (equations 2 and 3). Topological weight was represented by node degree centrality, while EoR indicated the extent to which drug treatment could revert gene expression from the disease state toward normal. A gene was considered effectively recovered if $EoR_{positive}$ (EoR > 0). Additionally, the Recovery Level (RL) was calculated using equation (4), cap-

turing the differential expression profile of each gene across normal, disease, and treatment groups.

$$NRI = RRODN_{all} + RRODN_{up} + RRODN_{down} \quad (1)$$

$$RRODN = W_{topo} \times EoR_{positive} \quad (2)$$

$$EoR = 100\% - |100\% - RL| \quad (3)$$

$$RL = \frac{\log_2(E_{treatment}) - \log_2(E_{disease})}{\log_2(E_{normal}) - \log_2(E_{disease})} \quad (4)$$

2.12. NTRA and pathway enrichment analysis

NTRA integrates topological properties (RankT) and transcriptomic properties (RankR) to identify key nodes in the T2DM liver-specific network. This algorithm relies on the relative ranking of parameters rather than their numerical values, as demonstrated in equations (5) to (7). In these equations, Rank denotes the relative ranking of parameters, while T, D, B, R, F, and P represent node parameters including topology, degree, betweenness, gene transcriptomics, fold change and *P*-value, respectively. For Kyoto Encyclopedia of Genes and Genomes (KEGG) pathway enrichment analysis using Metascape v3.5 (https://metascape.org), genes with EoR greater than 0 and ranked in the top 100 by NTRA were selected.

$$NTRA = Rank(RankT + RankR) \quad (5)$$

$$RankT = Rank(RankD + RankB) \quad (6)$$

$$RankR = Rank(RankF + RankP) \quad (7)$$

2.13. Target prediction and a "herb-ingredient-target-pathway" network construction

The ingredient targets were identified through the integration of HERB [24] (http://herb.ac.cn/) and BATMAN-TCM [25] (http://bionet.ncpsb.org.cn/batman-tcm/index.php) databases, along with the top 100 NTRA-ranked genes demonstrating effective recovery (EoR > 0). KEGG pathway enrichment analysis was conducted using Metascape v3.5. The "herb-ingredient-target-pathway" network was developed using Cytoscape (v3.82). Network topological properties, including degree and betweenness centrality of each node, were calculated using the NetworkAnalyzer plugin in Cytoscape.

2.14. Molecular docking

The protein and ingredient structures utilized in this study were obtained from the RCSB Protein Data Bank (http://www.rcsb.org) and PubChem (https://pubchem.ncbi.nlm.nih.gov/), respectively. The molecular docking analysis was performed using Autodock Vina (v1.1.2). Protein-ingredient interactions were visualized using PyMol (v2.1.0).

2.15. Western blot detection of hepatic phospho (p)-adenosine 5′-monophosphate-activated protein kinase α (p-AMPKα), AMPKα, p-acetyl-CoA carboxylase (p-ACC), and ACC protein expression

Hepatic tissue was homogenized and lysed in radio-immunoprecipitation assay lysis buffer containing 1% phenylmethanesulfonyl fluoride. Total protein concentration in the extracts was quantified using a Pierce BCA Protein Assay Kit (23225, Thermo Fisher, USA). The samples underwent electrophoresis in 10% TGX stain-free precast polyacrylamide gel before transfer to polyvinylidene difluoride (PVDF) membranes. The PVDF membranes were blocked in 5% BSA for 1 h, then incubated with primary antibodies AMPKα (5832S), p-AMPKα (Thr172) (2535S), ACC (3662S), p-ACC (Ser79) (3661S), and glyceraldehyde 3-phosphate dehydrogenase (GAPDH) (5174S) overnight at 4 °C, followed by incubation with goat anti-rabbit IgG conjugated to horseradish peroxidase (HRP) (Beyotime Biotechnology, Shanghai, China) (A0181) at room temperature for 2 h. The primary antibodies for AMPKα, p-AMPKα, ACC, p-ACC, and GAPDH were sourced from Cell Signaling Technology. Subsequently, Immobilon™ Western chemiluminescent HRP substrate (Millipore) was applied, and protein bands were measured using ChemiDoc Imaging Systems (Bio-Rad, California, USA).

2.16. Statistical analysis

All data were expressed as mean ± standard deviation (SD). GraphPad Prism 9 software was employed for data analysis and visualization. Group differences were analyzed using one-way ANOVA and Dunnett's test in GraphPad Prism 9 software, with $P < 0.05$ indicating statistical significance.

3. Results

3.1. Chemical profiling of total alkaloids from Coptis chinensis and total ginsenosides from Panax ginseng

Ultra-high performance liquid chromatography-triple quadrupole time-of-flight mass spectrometry (UPLC-Triple-TOF/MS) was utilized to systematically characterize the chemical profiling of total alkaloids from *Coptis chinensis* and total ginsenosides from *Panax ginseng*. The total ion chromatograms are shown in Figs. S1 and S2. The analysis identified 48 ingredients, including berberine, palmatine, ginsenoside Re, ginsenoside Rg1, and ginsenoside Rf (Table S1 and S2).

3.2. Effects of different compatibility ratios of total alkaloids from Coptis chinensis and total ginsenosides from Panax ginseng on gluconeogenesis and insulin resistance in primary mouse hepatocytes

Primary hepatocytes exhibit biological characteristics and functions similar to hepatocytes *in vivo*, making them the gold standard for *in vitro* studies of liver diseases and drug therapy [26]. Initially, the effects of total alkaloids from *Coptis chinensis* and total ginsenosides from *Panax ginseng* on primary mouse hepatocyte viability were assessed using the CCK8 assay. As demonstrated in Fig. 1A, total alkaloids from *Coptis chinensis* exhibited toxicity to primary hepatocytes at 40 μg raw medicinal herbs·mL^{-1}, while showing no significant cytotoxic effects at lower concentrations (0–20 μg raw medicinal herbs·mL^{-1}). Total ginsenosides from *Panax ginseng* demonstrated no impact on primary mouse hepatocyte viability at concentrations up to 40 μg raw medicinal herbs·mL^{-1} (Fig. 1B). Subsequently, the total concentration of both compounds was established at 20 μg raw medicinal herbs·mL^{-1}. The total alkaloids from *Coptis chinensis* and total ginsenosides from *Panax ginseng* were evaluated at ratios of 0∶1, 1∶4, 1∶2, 1∶1, 2∶1, 4∶1, and 1∶0 to examine their combined cytotoxicity on primary mouse hepatocytes. As illustrated in Fig. 1C, none of these combinations demonstrated significant cytotoxic effects. Therefore, the total concentration of 20 μg raw medicinal herbs·mL^{-1} with geometric baseline ratios of 0∶1, 1∶4, 1∶2, 1∶1, 2∶1, 4∶1, and 1∶0 was selected for subsequent cell experiments.

Excessive gluconeogenesis represents a key factor contributing to elevated FBG in T2DM [27]. An *in vitro* model of hepatic gluconeogenesis was established by treating primary mouse hepatocytes with 100 nmol·L^{-1} glucagon for 6 h to induce abnormal elevation of gluconeogenesis. With the exception of group 1 (0∶1 ra-

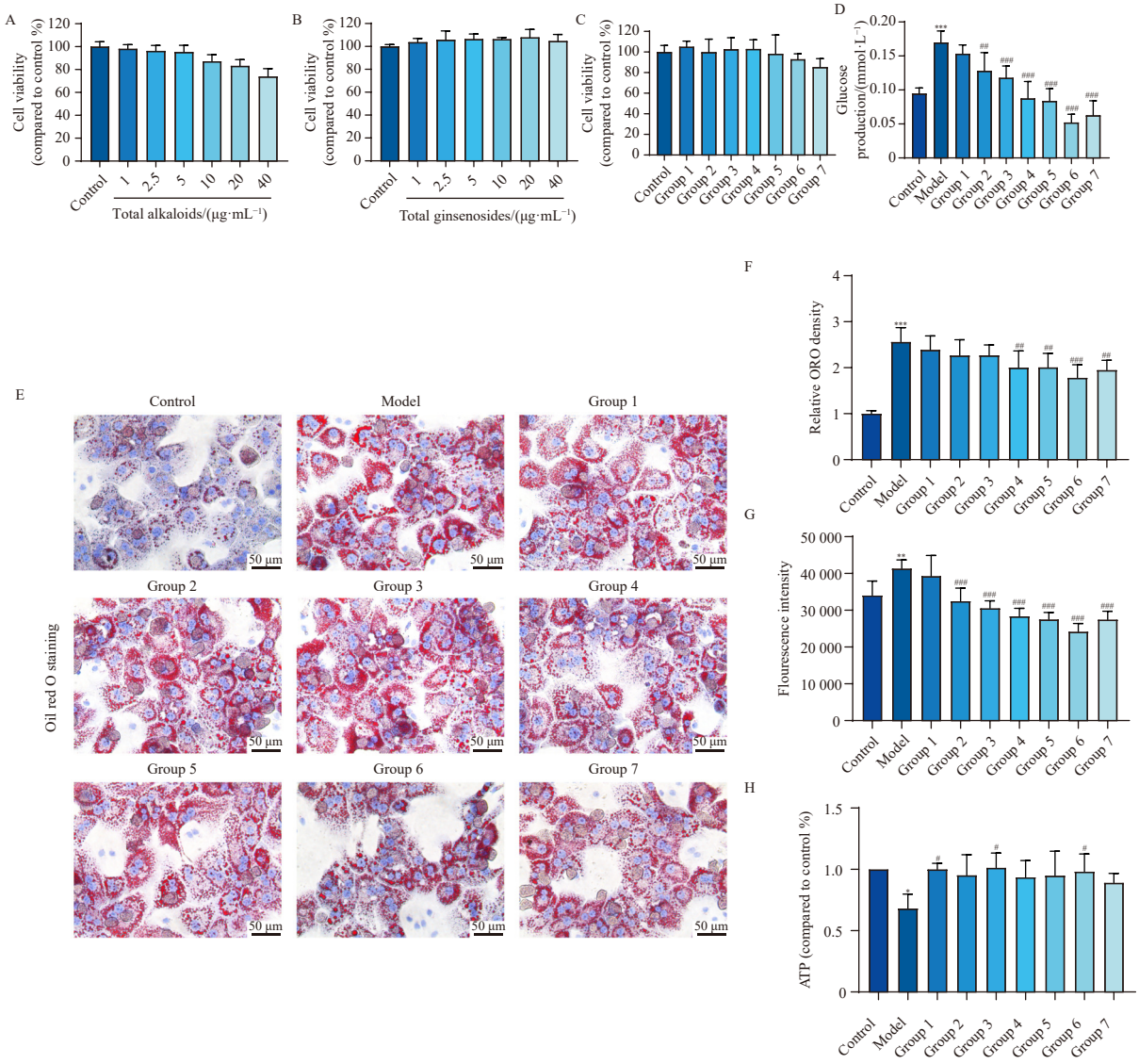

Fig. 1 Effects of different proportions of total alkaloids from *Coptis chinensis* and total ginsenosides from *Panax ginseng* on primary mouse hepatocytes. (A, B) Effects of total alkaloids from *Coptis chinensis* (A) and total ginsenosides from *Panax ginseng* (B) at different concentrations on the survival rate of primary mouse hepatocytes. (C–H) Effects of different proportions of total alkaloids from *Coptis chinensis* and total ginsenosides from *Panax ginseng* on cell viability (C), gluconeogenesis (D), lipid accumulation (E and F, 200 ×, Scale bar = 50 μm), oxidative stress (G), and ATP production (H) in primary mouse hepatocytes. Group 1 (0∶1 ratio of total alkaloids from *Coptis chinensis* and total ginsenosides from *Panax ginseng*), Group 2 (1∶4), Group 3 (1∶2), Group 4 (1∶1), Group 5 (2∶1), Group 6 (4∶1), Group 7 (1∶0). The results were expressed as mean ± SD. Values were from three independent experiments. $^{*}P < 0.05$, $^{**}P < 0.01$, $^{***}P < 0.001$ *vs* Control; $^{\#}P < 0.05$, $^{\#\#}P < 0.01$, $^{\#\#\#}P < 0.001$ *vs* Model.

tio of total alkaloids from *Coptis chinensis* and total ginsenosides from *Panax ginseng*), the glucose concentration in the cell supernatant of the 1∶4, 1∶2, 1∶1, 2∶1, 4∶1, and 1∶0 groups was significantly lower than that of the model group (Fig. 1D). The 4∶1 ratio demonstrated optimal suppression of hepatocyte gluconeogenesis, followed by the 1∶0 ratio group.

To evaluate the effects of varying compatibility ratios between total alkaloids from *Coptis chinensis* and total ginsenosides from *Panax ginseng* on lipid accumulation, oxidative stress, and mitochondrial dysfunction in hepatocytes under metabolic stress conditions, primary mouse hepatocytes treated with palmitic acid/oleic acid (PO) served as the cell model. Oil Red O staining revealed that treatments with compatibility ratios of 1∶1, 2∶1, 4∶1, and 1∶0 significantly decreased PO-induced lipid droplet formation (Figs. 1E and 1F). As indicated in Fig. 1G, PO exposure elevated intracellular reactive oxygen species levels in primary mouse hepatocytes ($P < 0.01$), which was substantially inhibited by various proportions of total alkaloids from *Coptis chinensis* and total ginsenosides from *Panax ginseng*. Compared to the control group, adenosine 5'-triphosphate (ATP) production in primary hepatocytes of the model group was significantly inhibited, indicating PO-induced mitochondrial dysfunction (Fig. 1H). Compared to the model group, ATP production was significantly restored by groups 1 (0∶1, $P < 0.05$), 3 (1∶2, $P < 0.05$), and 6 (4∶1, $P < 0.05$). These results demonstrated that the compatibility of total alkaloids from *Coptis chinensis* and total ginsenosides from *Panax ginseng* at a 4∶1 ratio exhibited optimal effects in improving hepatocyte insulin resistance and gluconeogenesis, showing significant inhibition of gluconeogenesis, reduction of intracellular lipid accumulation and oxidative stress, and enhancement of ATP production in primary hepatocytes.

3.3. In vivo anti-diabetic activity of total alkaloids from Coptis chinensis and total ginsenosides from Panax ginseng with the ratio of 4∶1

Mouse body weight was measured weekly. As shown in Fig. 2A, from the 0th to the 8th week of administration, the body weight of the db/db model group ($P < 0.001$) was significantly higher than that of the db/m control group. Following administration, mice in the HL group ($P < 0.01$) and HLRS group ($P < 0.01$) showed significant weight reduction compared to the

db/db model group. However, the body weight in the RS group ($P > 0.05$) and Met group ($P > 0.05$) showed no significant difference from the db/db model group. As illustrated in Figs. 2B–2D, the ratio of iWAT, eWAT, and pWAT to body weight increased substantially in T2DM mice. After 8 weeks of treatment with a 4∶1 ratio of total alkaloids from *Coptis chinensis* and total ginsenosides from *Panax ginseng*, the relative amounts of eWAT, iWAT, and pWAT decreased significantly. Notably, administration of total alkaloids from *Coptis chinensis* or total ginsenosides from *Panax ginseng* alone showed lesser effects on white adipose tissue relative amounts. Total alkaloids from *Coptis chinensis* influenced changes in relative levels of eWAT and iWAT, while total ginsenosides from *Panax ginseng* only affected the relative level of eWAT.

The FBG levels across groups after 8 weeks of drug intervention are presented in Fig. 3A. FBG levels were significantly elevated in the db/db group compared to those in the db/m group but were notably reduced in the RS group, HL group, and HLRS group. These findings suggest that total alkaloids from *Coptis chinensis* and total ginsenosides from *Panax ginseng*, administered either individually or in combination, demonstrated anti-hyperglycemic effects in T2DM mice. Glucose tolerance was evaluated using the GTT assay. As shown in Figs. 3B and 3C, following intraperitoneal glucose injection, the AUC of GTT assay was significantly higher in the db/db model group compared to the db/m control group ($P < 0.001$), indicating substantial glucose resistance. The results demonstrated that total alkaloids from *Coptis chinensis* and total ginsenosides from *Panax ginseng*, alone or combined, enhanced glucose clearance in T2DM mice and effectively normalized the AUC value. Additionally, PAS staining of liver sections revealed that drug intervention partially restored the depleted hepatic glycogen content in db/db mice (Fig. 3D).

To examine the effects of drug interventions on insulin sensitivity in db/db mice, an ITT assay was performed one week after the GTT assay. The findings indicated that insulin efficacy was substantially reduced in db/db mice compared to db/m mice, particularly during initial insulin administration. However, total alkaloids from *Coptis chinensis* and total ginsenosides from *Panax ginseng*, individually or combined, enhanced insulin efficiency in db/db mice (Figs. 3E and 3F). Notably, the HOMA-IR was significantly elevated in the db/db model group compared to the db/m control group ($P < 0.001$), confirming insulin resistance in db/db mice (Fig. 3G). Following eight weeks of drug intervention, HOMA-IR values in the RS group, HL group, and HLRS group were significantly reduced compared to the db/db model group. These findings collectively demonstrate that total alkaloids from *Coptis chinensis* and total ginsenosides from *Panax ginseng*, alone or combined, significantly improved glucose metabolism and insulin resistance in db/db mice.

Lipid metabolism abnormalities frequently occur in T2DM patients. In this study, db/db mice exhibited diabetic dyslipidemia, characterized by elevated serum levels of TC, TG, LDL-C, and reduced HDL-C compared to db/m mice (Figs. 4A–4D). After 8 weeks of drug administration, serum TC, TG, and LDL-C levels were significantly reduced in the HL group and HLRS group, while HDL-C levels increased significantly in the RS group. H&E staining revealed normal liver tissue architecture in db/m mice, with intact hepatic lobules and organized hepatocytes. In contrast, db/db mice exhibited steatosis, hepatocyte swelling, and hepatocellular ballooning (Fig. 4E). Following 8 weeks of drug intervention, liver conditions improved in all treatment groups compared to the db/db model group, with the HLRS group showing the most pronounced improvement. Oil red O staining confirmed substantial lipid accumulation with large, dense lipid droplets in the db/db model group. Consistent with H&E findings, after 8 weeks of treatment, total alkaloids from *Coptis chinensis* and total ginsenosides from *Panax ginseng*, alone or combined, reduced hepatic lipid accumulation in T2DM mice, with the HLRS group demonstrating the most significant improvement (Fig. 4E).

3.4. Synergistic effect of total alkaloids from *Coptis chinensis* and total ginsenosides from *Panax ginseng* in the treatment of T2DM

The results demonstrated that the HLRS group exhibited superior efficacy compared to groups receiving either total alkaloids from *Coptis chinensis* or total ginsenosides from *Panax ginseng* alone across multiple pharmacotherapeutic indicators. To elucidate the synergistic effect of combining total alkaloids from *Coptis chinensis* and total ginsenosides from *Panax ginseng*, the combined index (CI) value was calculated using the Bliss independence model. Fig. 5 illustrates that the CI values for total alkaloids from *Coptis chinensis* and total ginsenosides from *Panax ginseng* regarding FBG, the ratio of eWAT to body weight, AUC of GTT, and HOMA-IR were 0.8114, 0.8212, 0.7156, and 0.7113, respectively, with all *P*-values below 0.05. These findings collectively indicate that the 4∶1 combination of total alkaloids from *Coptis chinensis* and total ginsenosides from *Panax ginseng* demonstrates significant synergistic anti-diabetic effects *in vivo*.

3.5. RNA-seq analysis and T2DM liver-specific network construction

Having established that the 4∶1 combination of total alkaloids from *Coptis chinensis* and total ginsenosides from *Panax ginseng* exhibited synergistic anti-diabetic effects in db/db mice, further investigation into the underlying mechanism was conducted using a combined approach of network pharmacology and transcriptomics. Initially, RNA-seq analysis was performed on liver tissue from mice treated with total alkaloids from *Coptis chinensis* and total ginsenosides from *Panax ginseng*, both individually and in combination, over an 8-week period.

A total of 810 T2DM-related genes expressed in the liver were obtained by integrating the data from the GeneCard database, the HPA, and our RNA-seq dataset. These genes were used to construct a PPI network specific to T2DM liver pathology, which was visualized using Cytoscape. The largest connected component within this network, comprising 337 nodes and 781 edges, was defined as the T2DM liver-specific network (Fig. 6A). In the db/db model group, gene expression in liver tissues

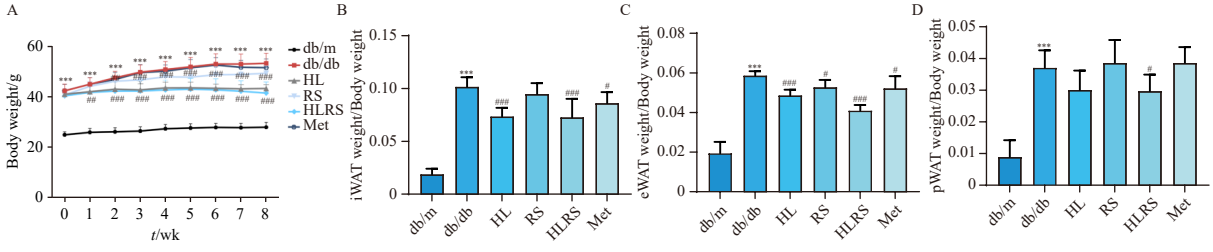

Fig. 2 Effects of total alkaloids from *Coptis chinensis*, total ginsenosides from *Panax ginseng*, and their combination (4∶1) on body weight and organ coefficients in T2DM mice. (A) The body weight per week. (B–D) The weight ratio of iWAT, eWAT, or pWAT to body weight after 8 weeks of administration. The results were expressed as mean ± SD ($n = 6$ or 12 for each group). $^{***}P < 0.001$ *vs* db/m control group; $^{\#}P < 0.05$, $^{\#\#}P < 0.01$, $^{\#\#\#}P < 0.001$ *vs* db/db model group.

showed significant alterations. As illustrated in Fig. 6B, nodes within the network were color-coded according to the fold change in expression between db/db mice and db/m controls, with red indicating up-regulation and green indicating down-regulation. Following drug intervention, nodes were recolored based on their EoR values to represent the extent of gene expression normalization (Figs. 6C–6E). The combination of total alkaloids from *Coptis chinensis* and total ginsenosides from *Panax ginseng* demonstrated the most substantial regulation of the T2DM liver-specific network under diabetic conditions (Fig. 6E), while total ginsenosides from *Panax ginseng* alone showed minimal regulation (Fig. 6D).

3.6. Evaluation of the efficacy and synergistic effect of the 4∶1 combination of total alkaloids from Coptis chinensis and total ginsenosides from Panax ginseng using NRI

To quantitatively evaluate drug efficacy from the perspective

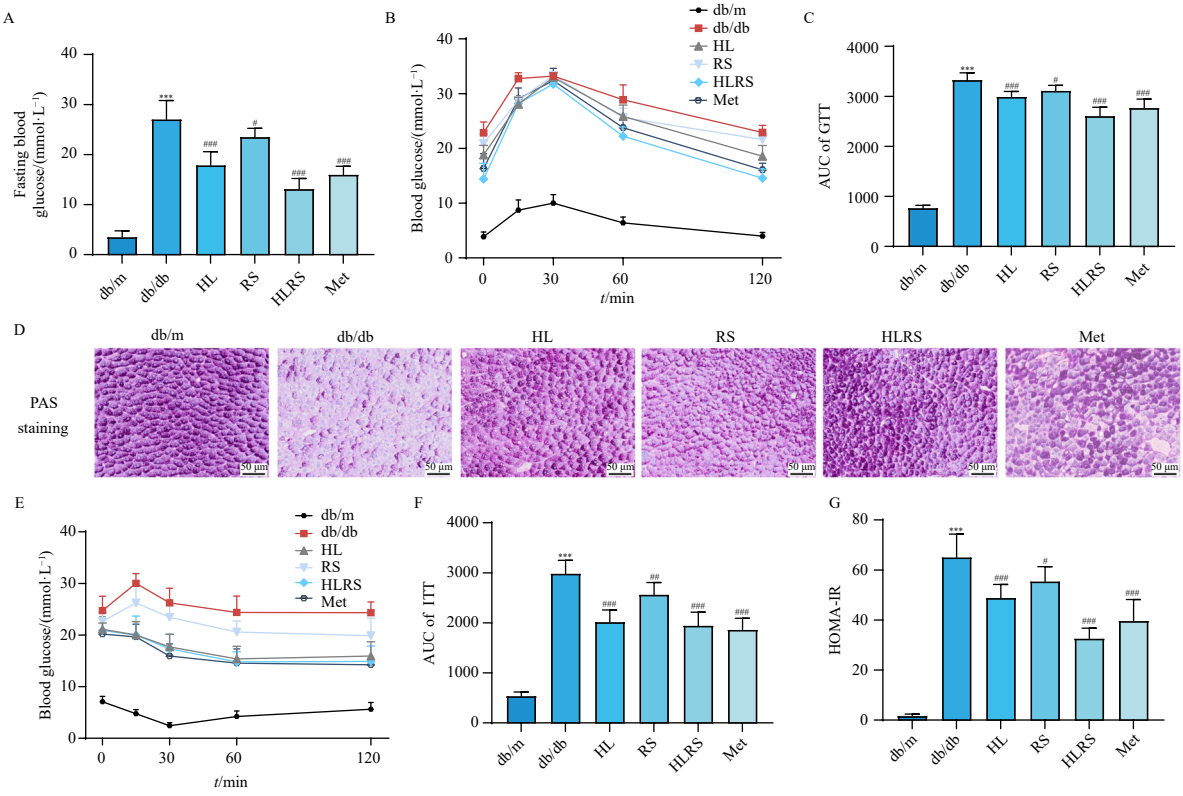

Fig. 3 Effects of total alkaloids from *Coptis chinensis*, total ginsenosides from *Panax ginseng,* and their combination (4∶1) on glucose metabolism and insulin resistance in T2DM mice. (A) Fasting blood glucose (FBG). (B) Glucose tolerance determined by GTT. (C) Quantification of the AUC of the GTT. (D) Hepatic glycogen accumulation was evaluated by PAS staining (200 ×, Scale bar = 50 μm) from three mice. (E) Insulin tolerance determined by ITT. (F) Quantification of the AUC of the ITT. (G) HOMA-IR. The results were expressed as mean ± SD (n = 6 or 12 for each group). $^{***}P < 0.001$ *vs* db/m control group; $^{\#}P < 0.05$, $^{\#\#}P < 0.01$, $^{\#\#\#}P < 0.001$ *vs* db/db model group.

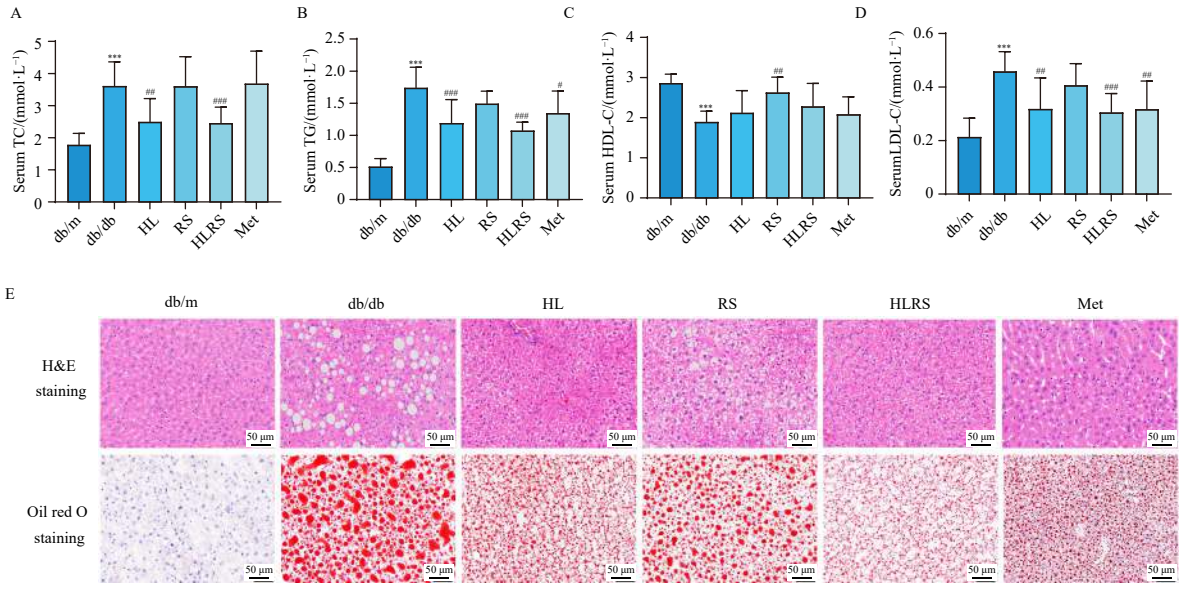

Fig. 4 Effects of total alkaloids from *Coptis chinensis*, total ginsenosides from *Panax ginseng,* and their combination (4∶1) on lipid metabolism in T2DM mice. (A) serum TC. (B) serum TG. (C) serum HDL-C. (D) serum LDL-C. (E) Hepatic pathological changes were evaluated by H&E staining (200 ×, scale bar = 50 μm) and oil red O staining (200 ×, scale bar = 50 μm) from three mice. The results were expressed as mean ± SD (n = 6 or 12 for each group). $^{***}P < 0.001$ *vs* db/m control group; $^{\#}P < 0.05$, $^{\#\#}P < 0.01$, $^{\#\#\#}P < 0.001$ *vs* db/db model group.

of disease-related biological network balance, the NRI score was calculated for total alkaloids from *Coptis chinensis* and total ginsenosides from *Panax ginseng*, both alone and in combination, on the T2DM liver-specific network (Table 1). The combined treatment yielded the highest NRI score of 389.46, with contribution values of 59.85, 62.89, and 266.72 for significantly up-regulated nodes, significantly down-regulated nodes, and all nodes in the T2DM liver-specific network, respectively. Total alkaloids from *Coptis chinensis* achieved an NRI score of 347.63, exceeding that of total ginsenosides from *Panax ginseng* at 154.69. These findings demonstrated that the combination treatment exhibited superior recovery performance on the T2DM liver-specific network, followed by total alkaloids from *Coptis chinensis* alone, while total ginsenosides from *Panax ginseng* alone showed the least effective recovery, consistent with their anti-diabetic effects *in vivo*.

A randomization test was conducted to assess the significance of recovery effects from the single or combined administration of total alkaloids from *Coptis chinensis* and total ginsenosides from *Panax ginseng* on the T2DM liver-specific network. The NRI for each randomization test was calculated by simulating the RL based on a normal distribution and repeated 10 000 times. One sample *t*-test analysis was employed for statistical analysis of simulated NRI values and the NRI value after drug intervention. The results indicated that the recovery effects of both individual and combined treatments on the T2DM liver-specific network were significantly higher than their corresponding randomization tests ($P < 2.2 \times 10^{-16}$).

3.7. Pathway enrichment analysis based on NTRA and EoR

To investigate the pharmacological mechanism of total alkaloids from *Coptis chinensis* and total ginsenosides from *Panax ginseng* in treating T2DM and their synergistic effects, NTRA and EoR methods were utilized to identify key disease nodes with recovery regulatory responses for pathway enrichment analysis. The analysis identified 47, 22, and 54 nodes ranking in the top 100 in NTRA with effective recovery (EoR > 0) after administration in the total alkaloids from *Coptis chinensis*, total ginsenosides from *Panax ginseng*, and their combination groups, respectively (Fig. 7A). Pathway enrichment analysis was subsequently performed using Metascape to compare their potential pharmacological mechanisms. The enrichment results (Fig. 7B) showed that the HL group, RS group, and their combination HLRS group were enriched into 19, 7, and 20 clusters, respectively. The HL group showed significant enrichment in thyroid hormone signaling pathway ($Q = 3.33 \times 10^{-10}$), mitophagy ($Q = 2.45 \times 10^{-5}$), mitogen-activated protein kinase (MAPK) signaling pathway ($Q = 3.43 \times 10^{-5}$), while the estrogen signaling pathway ($Q = 1.78 \times 10^{-3}$) was highly enriched in the RS group. The therapeutic effect of the combined administration may be attributed to its regulation of energy metabolism and inflammation response, as evidenced by significant enrichment in the AMPK signaling pathway ($Q = 7.98 \times 10^{-7}$), neutrophil extracellular trap formation ($Q = 9.04 \times 10^{-6}$), MAPK signaling pathway ($Q = 8.08 \times 10^{-4}$), and HIF-1 signaling pathway ($Q = 1.05 \times 10^{-5}$) in the HLRS group. These findings indicate distinct mechanisms of action when the compounds are administered alone or in combination.

To examine the synergistic mechanism of total alkaloids from *Coptis chinensis* and total ginsenosides from *Panax ginseng*, 52 nodes ranking in the top 100 in NTRA with stronger effective recovery in the HLRS group compared to HL or RS groups were analyzed, resulting in enrichment of 20 KEGG pathway clusters (Fig. 7C). Excluding human disease pathways unrelated to T2DM, significant enhancement was observed in the AMPK signaling pathway ($Q = 6.34 \times 10^{-7}$), HIF-1 signaling pathway ($Q = 8.83 \times 10^{-6}$), cellular senescence ($Q = 4.21 \times 10^{-5}$), cholesterol metabolism ($Q = 4.05 \times 10^{-4}$), and JAK-STAT signaling pathway ($Q = 7.89 \times 10^{-4}$).

3.8. The "herb-ingredient-target-pathway" network construction and molecular docking

Using UPLC-Triple-TOF/MS analysis, 48 ingredients were identified, including berberine, palmatine, ginsenoside Re, ginsenoside Rg1, and ginsenoside Rf. Based on the absorption potential of chemical ingredients into the bloodstream after oral administration, the potential active ingredients of total alkaloids from *Coptis chinensis* were identified as berberine, palmatine, coptisine, epiberberine, jatrorrhizine, and columbamine [28-31]. For total ginsenosides from *Panax ginseng*, the potential active ingredients comprised ginsenoside Re, Rg1, Rf, Rb1, Rc, Rg2, Rh1, F1, Rd, F2, Rg3, Rh2, Rb2, and compound K [32-35]. Through the integration of 208 database targets and 73 key nodes from the T2DM liver-specific network, 260 targets of potential active ingredients were identified, including 21 overlapping targets (Fig. S3). Pathway enrichment analysis of all 260 targets revealed 96 KEGG pathways with *Q* values below 1×10^{-15}. A "herb-ingredient-target-pathway" network comprising 321 nodes and 3464 edges was constructed using Cytoscape to illustrate the interactions among 2 herbs, 20 ingredients, 203 targets, and 96 KEGG pathways (Fig. 8A). As illustrated in Figs. 8A and S4, the 10 pathways in the middle circle were also enriched by the 21 overlapping targets and represented key KEGG pathway clusters. Among these, insulin resistance, AMPK signaling pathway, and HIF-1 signaling pathway demonstrated clear associations with T2DM.

Based on network topological properties (degree and betweenness centrality), relative contents of active ingredients, and significantly enriched pathways associated with T2DM, 10 active ingredients and 19 target proteins (Table S3) were selected for molecular docking. As demonstrated in Figs. 8B and 8C, the binding energies of protein-ingredient complexes were all below −5.4 kcal·mol^{-1}, indicating strong affinities between the active ingredients and these target proteins.

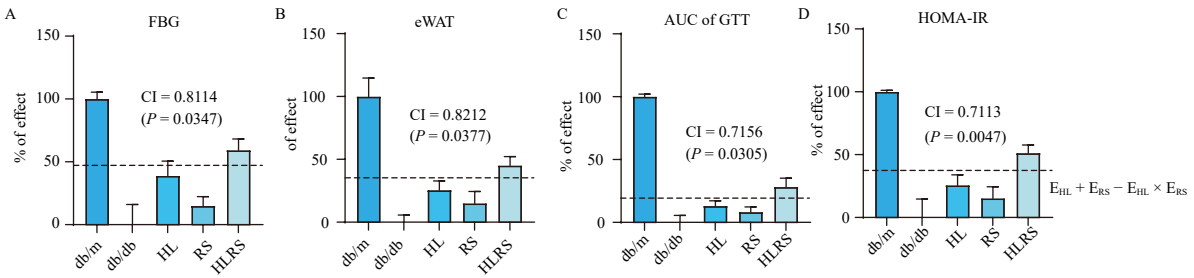

Fig. 5 Total alkaloids from *Coptis chinensis* and total ginsenosides from *Panax ginseng* exhibited synergistic effects in the treatment of T2DM. Statistical diagram of the combination index (CI) on fasting blood glucose (A), the ratio of eWAT to body weight (B), AUC of GTT (C), and HOMA-IR (D). CI = $(E_{HL} + E_{RS} - E_{HL} \times E_{RS})/E_{HLRS}$. The results were expressed as mean ± SD (n = 6 or 12 for each group). The dashed line represented the expected additive effect value, denoted as $E_{HL} + E_{RS} - E_{HL} \times E_{RS}$. The statistical significance between E_{HLRS} and the expected additive effect value was measured using the Student's *t*-test.

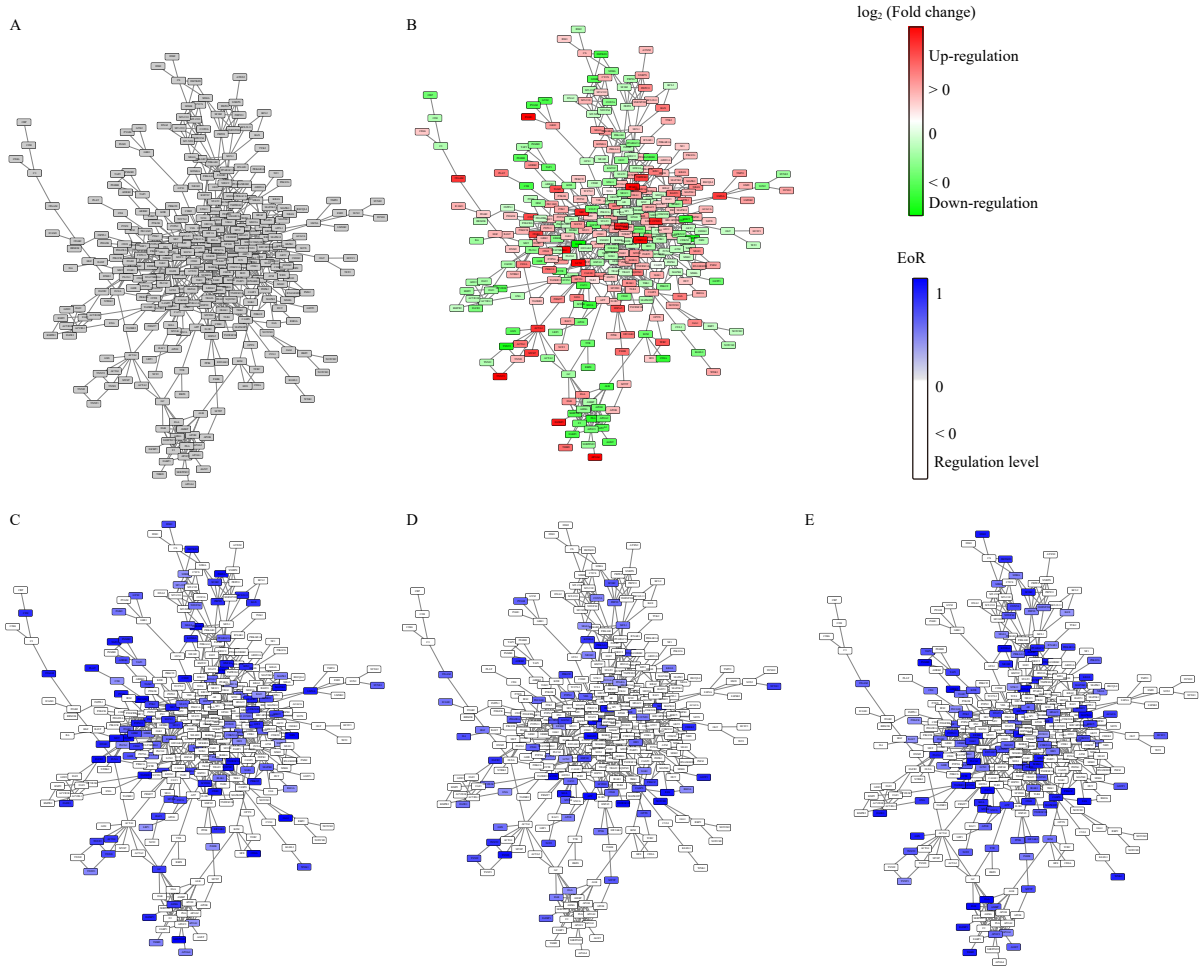

Fig. 6 T2DM liver-specific network under different conditions. (A) T2DM liver-specific network. Nodes were liver-specific targets of T2DM, and edges were their protein-protein interactions (PPIs). (B) T2DM liver-specific disturbed network. Green nodes represented down-regulated genes [$\log_2(E_{disease}) - \log_2(E_{normal})] < -0.5$ after diseases, while red nodes represented up-regulated genes [$\log_2(E_{disease}) - \log_2(E_{normal})] > 0.5$. (C–E) The recovery regulation effects (EoR) of total alkaloids from *Coptis chinensis* (C), total ginsenosides from *Panax ginseng* (D), and their combination (E) on T2DM liver-specific network. The color of the node represented the EoR value. The maximum EoR value is 1, and the darker the blue, the closer it is to 1.

Table 1 The NRI results (mean ± SD, n = 10 000).

	HL	RS	HLRS
$RRODN_{all}$	246.19	118.32	266.72
$RRODN_{up}$	54.76	24.17	59.85
$RRODN_{down}$	46.68	12.20	62.89
NRI	347.63	154.69	389.46
$NRI_{randomization}$	88.90 ± 27.97	67.61 ± 24.92	44.27 ± 20.02
P-value	$< 2.2 \times 10^{-16}$	$< 2.2 \times 10^{-16}$	$< 2.2 \times 10^{-16}$

3.9. Validation of key proteins in the AMPK signaling pathway

Western blot analysis was employed to validate the network analysis results by determining the protein expression levels of key proteins in the AMPK signaling pathway in mouse liver tissue. The analysis revealed that the relative expressions of p-AMPKα/AMPKα and p-ACC/ACC were significantly decreased in the db/db model group compared to the db/m control group (Fig. 9). The total alkaloids from *Coptis chinensis* and total ginsenosides from *Panax ginseng* enhanced the expression levels of p-AMPKα/AMPKα and p-ACC/ACC to varying degrees. Notably, the combination group (HLRS) demonstrated the most substantial improvement, suggesting that the compatibility of total alkaloids from *Coptis chinensis* and total ginsenosides from *Panax ginseng* produces a synergistic therapeutic effect on T2DM through the AMPK signaling pathway.

4. Discussion

T2DM represents an increasingly severe global health challenge, with rising prevalence and incidence among individuals under 20 years of age [36]. *Coptis chinensis* and *Panax ginseng* have demonstrated anti-hyperglycemic properties [37, 38]. However, the regulatory mechanisms underlying the combined effects of *Coptis chinensis* and *Panax ginseng* on T2DM remain incompletely understood. This study investigated the synergistic effects of these two medicinal plants on T2DM and their potential mechanisms through the integration of *in vivo* experiments, network pharmacology, and molecular docking. The findings revealed an optimal ratio of 4∶1 between total alkaloids from *Coptis chinensis* and total ginsenosides from *Panax ginseng*. Following 8 weeks of either single or combined (4∶1) administration of total alkaloids from *Coptis chinensis* and total ginsenosides from *Panax ginseng*, db/db mice exhibited improved FBG and HOMA-IR levels through the regulation of hepatic glucose and lipid metabolism, with the 4∶1 combination showing superior efficacy. Furthermore, the CI values of FBG, the ratio of eWAT to body weight, AUC of GTT, and HOMA-IR provided strong evidence for the significant synergistic anti-diabetic effect of the 4∶1 combination *in vivo*.

Multi-target and multi-pathway mechanisms characterize the efficacy of TCM [39]. Hepatic insulin resistance [40], excessive glucon-

eogenesis [41, 42], and lipid accumulation [43] are commonly observed in T2DM patients. This study integrated transcriptomics with network pharmacology to establish a T2DM liver-specific network, enabling further investigation of the synergistic anti-diabetic effects and potential pharmacological mechanisms of the combined administration. The NRI scores calculated on the T2DM liver-specific network confirmed superior efficacy of the combined administration compared to individual treatments from a biomolecular network perspective. The integration of NTRA and EoR methods identified key nodes associated with therapeutic effects. The analysis revealed 31 nodes effectively regulated by both HL and HLRS groups, with HLRS demonstrating stronger regulatory effects on 21 of these nodes. Additionally, distinct regulatory patterns emerged, with HL regulating 16 specific nodes and HLRS regulating 23 specific nodes. Of the 17 nodes effectively regulated by both RS and HLRS groups, HLRS exhibited greater regulatory intensity in more than 75% of cases. Moreover, HLRS specifically regulated 37 nodes, while RS regulated only 5 nodes. These findings corroborated the animal experimental results, demonstrating HLRS's superior anti-diabetic effect, followed by HL, with RS showing the least efficacy.

Furthermore, a total of 39 KEGG pathway clusters related to pharmacological effects of HL, RS, or HLRS were enriched. The HL group exhibited significant enrichment in thyroid hormone signaling pathway, mitophagy, and MAPK signaling pathway, suggesting these pathways were primarily involved in the treatment of T2DM with total alkaloids from *Coptis chinensis*. Thyroid hormone has been implicated in insulin signaling and glucose homeostasis [44], while both hyperthyroidism and hypothyroidism increase the risk of developing different types of diabetes [45]. He et al. demonstrated that mitophagy, a crucial regulator of mitochondrial homeostasis, can lead to hepatic insulin resistance and T2DM [46]. The RS group showed high enrichment in the estrogen signaling pathway, indicating its significant contribution to the intervention of total ginsenosides from *Panax ginseng* in T2DM. Substantial evidence confirms that estrogen/ER signaling plays a vital role in glucose homeostasis and lipid metabolism [47]. Dysregulation of estrogen signaling or estrogen deficiency associates with insulin production, insulin resistance, and gluconeogenesis, contributing to diabetes development [48, 49]. The HLRS group showed prominence in pathways including the AMPK signaling pathway, neutrophil extracellular trap formation, the MAPK signaling pathway, and the HIF-1 signaling pathway. Neutrophil extracellular traps show elevation in T2DM individuals, contributing to the progression of diabetic complications [50, 51]. MAPKs play essential roles in the regulation of hepatic metabolic processes, including lipid metabolism and glucose homeostasis [52]. AMPK, functioning as a cellular energy sensor, represents a potential target for diabetes treatment [53, 54]. Notably, pathways such as the AMPK signaling pathway and the HIF-1 signaling pathway were enriched by 52 nodes. These nodes ranked in the top 100 of NTRA in the T2DM liver-specific network, with the HLRS group showing stronger effective recovery than the HL or RS group alone. These findings suggest that the combined treatment exerts synergistic anti-T2DM effects by enhancing the regulatory influence on multiple key pathways, particularly the AMPK signaling pathway and the HIF-1 signaling pathway.

To better elucidate the anti-T2DM mechanisms of the combined total alkaloids from *Coptis chinensis* and total ginsenosides from *Panax ginseng*, a "herb-ingredient-target-pathway" network was constructed based on potentially active ingredients absorbed into blood and their targets. The binding affinity and interaction between potential pivotal ingredients and target proteins received indirect demonstration through molecular docking. Furthermore, as evidenced by increased p-AMPKα/AMPKα and p-ACC/ACC ratios, our *in vivo* experiments demonstrated that the combined administration of total alkaloids from *Coptis chinensis* and total ginsenosides from *Panax ginseng* activated the AMPK signaling pathway, thereby enhancing insulin sensitivity in db/db mice. The results establish that this combination exerts synergistic anti-T2DM effects through multi-compound, multi-target, and multi-pathway mechanisms, with AMPK/ACC signaling pathway serving as one crucial mechanism.

5. Conclusion

In conclusion, this study demonstrates that the 4∶1 compatibility of total alkaloids from *Coptis chinensis* and total ginsenosides from *Panax ginseng* produces superior anti-T2DM effects compared to individual treatments, particularly showing significant synergistic effects on glucose metabolism and insulin resistance in db/db mice. The integration of network pharmacology and molecular docking provides novel insights into the pharmacological effects and underlying mechanisms of TCM compatibil-

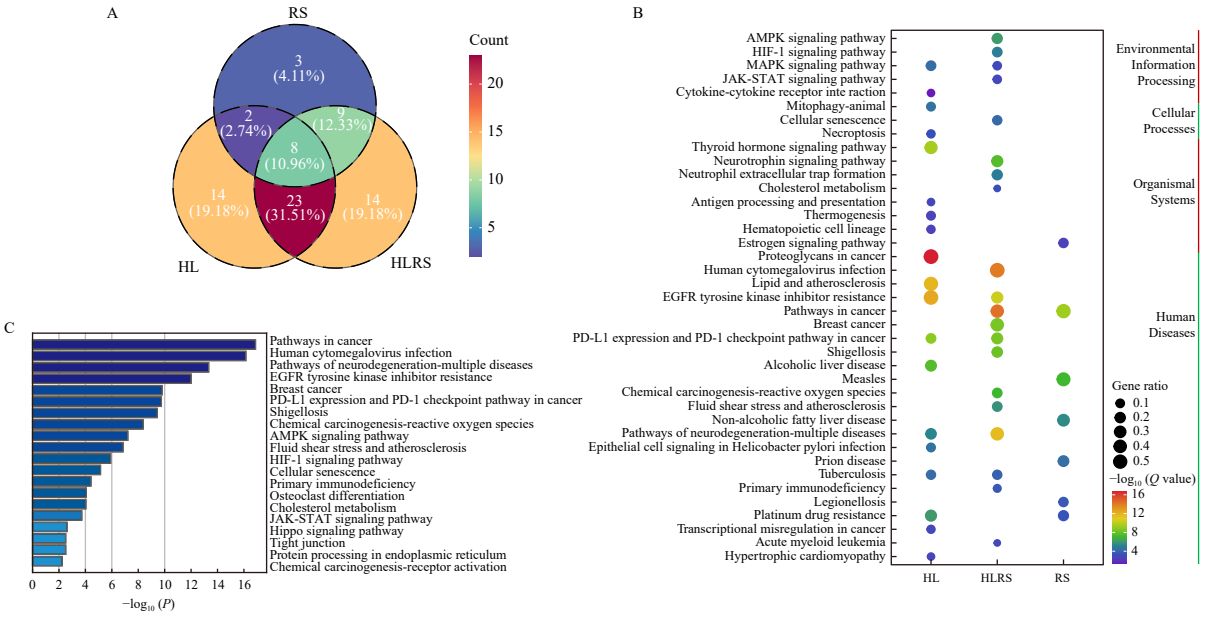

Fig. 7 Enriched pathway results. (A, B) Venn diagram (A) and KEGG pathway enrichment (B) of nodes that ranked in the top 100 in NTRA and showed effective recovery (EoR > 0) in HL, RS, and HLRS groups. The size and color of the dots represent the values of gene ratio and negative $\log_{10}$ (*Q* value), respectively. (C) KEGG pathway enrichment based on nodes that ranked in the top 100 in NTRA and displaying stronger effective recovery in the HLRS group compared to the HL or RS group.

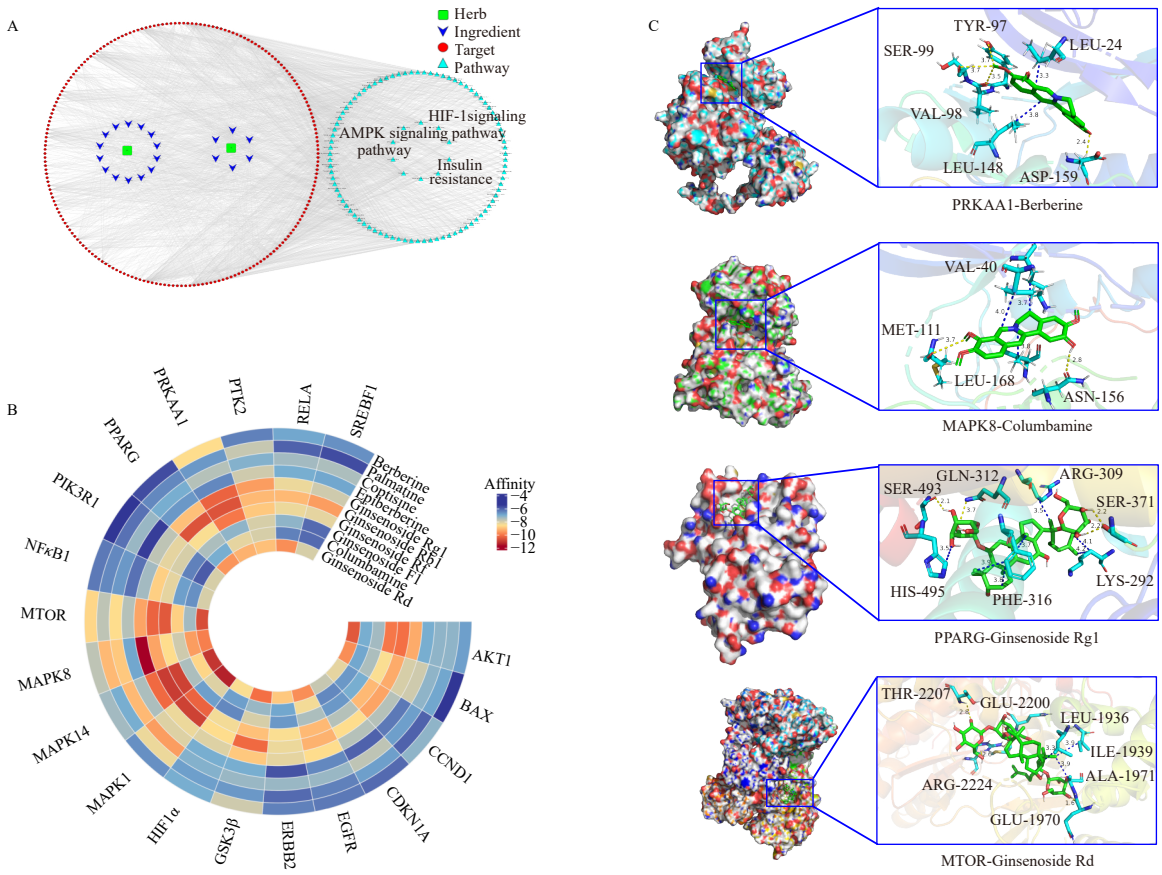

Fig. 8 Molecular docking between TCM ingredients and target proteins. (A) The "herb-ingredient-target-pathway" network. (B) The heatmap of binding energy between the 10 active ingredients and 19 target proteins. (C) The representative interaction diagrams of protein-ingredient complexes. The active site amino acid residues were represented as a cyan stick model, and the TCM ingredient was represented as a green stick model. The yellow and blue dotted lines represented hydrogen bonds and hydrophobic effects, respectively. Target proteins were indicated by their gene names.

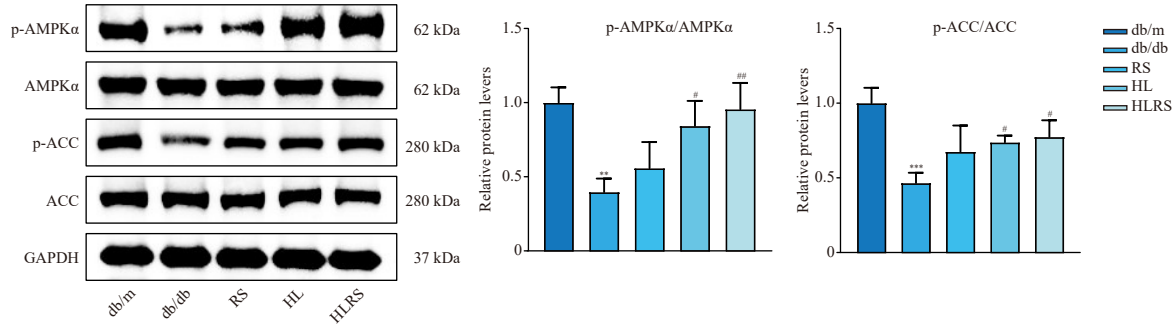

Fig. 9 Effects of total alkaloids from *Coptis chinensis*, total ginsenosides from *Panax ginseng*, and their combination (4∶1) on the hepatic p-AMPKα, AMPKα, p-ACC, and ACC protein expression in T2DM mice. The results were expressed as mean ± SD (n = 3). $^{**}P < 0.01$, $^{***}P < 0.001$ *vs* db/m control group; $^{\#}P < 0.05$, $^{\#\#}P < 0.01$ *vs* db/db model group.

ity. This study evaluates the holistic recovery effect of total alkaloids from *Coptis chinensis* and total ginsenosides from *Panax ginseng*, both individually and in combination, on T2DM liver-specific network, identifying AMPK/ACC signaling pathway as partially responsible for their synergistic therapeutic effect on T2DM.

Funding

This work was supported by the Pioneer and Leading Goose R&D Program of Zhejiang Province (No. 2024C03106), the National Natural Science Foundation of China (No. U23A20513), Ningbo Top Medical and Health Research Program (No. 2022030309), the Innovation Team and Talents Cultivation Program of the National Administration of Traditional Chinese Medicine (No. ZYYCXTD-D-202002).

Availability of supporting information

Supporting information for this study can be obtained by contacting the corresponding authors *via* E-mail.

Declaration of competing interest

All the authors declare that there is no conflict of interest for any of them.

Acknowledgments

The authors thank the High-Performance Computing Cluster of Zhejiang University Innovation Center of Yangtze River Delta for their technical support.

References

1 Ogurtsova K, Guariguata L, Barengo NC, et al. IDF Diabetes Atlas: global estimates of undiagnosed diabetes in adults for 2021. *Diabetes Res Clin Pract*. 2022;183:109118. https://doi.org/10.1016/j.diabres.2021.109118.

2 Dendup T, Feng X, Clingan S, et al. Environmental risk factors for developing type 2 diabetes mellitus: a systematic review. *Int J Environ Res Public Health*. 2018;15(1):78. https://doi.org/10.3390/ijerph15010078.

3 Wang L, Peng W, Zhao Z, et al. Prevalence and treatment of diabetes in China, 2013–2018. *JAMA*. 2021;326(24):2498-2506. https://doi.org/10.1001/jama.2021.22208.

4 Chan JCN, Lim LL, Wareham NJ, et al. The Lancet Commission on Diabetes: using data to transform diabetes care and patient lives. *Lancet*. 2021;396(10267):2019-2082. https://doi.org/10.1016/S0140-6736(20)32374-6.

5 Saeedi P, Salpea P, Karuranga S, et al. Mortality attributable to diabetes in 20–79 years old adults, 2019 estimates: results from the International Diabetes Federation Diabetes Atlas, 9th edition. *Diabetes Res Clin Pract*. 2020;162:108086. https://doi.org/10.1016/j.diabres.2020.108086.

6 Bianchi C, Daniele G, Dardano A, et al. Early combination therapy with oral glucose-lowering agents in type 2 diabetes. *Drugs*. 2017;77(3):247-264. https://doi.org/10.1007/s40265-017-0694-4.

7 Del Prato S. Rational combination therapy for type 2 diabetes. *Lancet Diabetes Endocrinol*. 2019;7(5):328-329. https://doi.org/10.1016/S2213-8587(19)30069-5.

8 Hu RF, Sun XB. Design of new traditional Chinese medicine herbal formulae for treatment of type 2 diabetes mellitus based on network pharmacology. *Chin J Nat Med*. 2017;15(6):436-441. https://doi.org/10.1016/s1875-5364(17)30065-1.

9 Wang H, Shi S, Wang S. Can highly cited herbs in ancient traditional Chinese medicine formulas and modern publications predict therapeutic targets for diabetes mellitus? *J Ethnopharmacol*. 2018;213:101-110. https://doi.org/10.1016/j.jep.2017.10.032.

10 Li JC, Shen XF, Meng XL. A traditional Chinese medicine JiuHuangLian (Rhizoma Coptidis steamed with rice wine) reduces oxidative stress injury in type 2 diabetic rats. *Food Chem Toxicol*. 2013;59:222-229. https://doi.org/10.1016/j.fct.2013.06.005.

11 Li JC, Shen XF, Shao JA, et al. The total alkaloids from *Coptis chinensis* Franch improve cognitive deficits in type 2 diabetic rats. *Drug Des Devel Ther*. 2018;12:2695-2706. https://doi.org/10.2147/DDDT.S171025.

12 Zhang H, Wei J, Xue R, et al. Berberine lowers blood glucose in type 2 diabetes mellitus patients through increasing insulin receptor expression. *Metabolism*. 2010;59(2):285-292. https://doi.org/10.1016/j.metabol.2009.07.029.

13 Zhang Y, Gu Y, Ren H, et al. Gut microbiome-related effects of berberine and probiotics on type 2 diabetes (the PREMOTE study). *Nat Commun*. 2020;11(1):5015. https://doi.org/10.1038/s41467-020-18414-8.

14 Sun Y, Xia M, Yan H, et al. Berberine attenuates hepatic steatosis and enhances energy expenditure in mice by inducing autophagy and fibroblast growth factor 21. *Br J Pharmacol*. 2018;175(2):374-387. https://doi.org/10.1111/bph.14079.

15 Zhao MM, Lu J, Li S, et al. Berberine is an insulin secretagogue targeting the KCNH6 potassium channel. *Nat Commun*. 2021;12(1):5616. https://doi.org/10.1038/s41467-021-25952-2.

16 Liu C, Zhang M, Hu MY, et al. Increased glucagon-like peptide-1 secretion may be involved in antidiabetic effects of ginsenosides. *J Endocrinol*. 2013;217(2):185-196. https://doi.org/10.1530/JOE-12-0502.

17 Liu Q, Zhang FG, Zhang WS, et al. Ginsenoside Rg1 inhibits glucagon-induced hepatic gluconeogenesis through Akt-FoxO1 interaction. *Theranostics*. 2017;7(16):4001-4012. https://doi.org/10.7150/thno.18788.

18 Zhou R, He D, Zhang H, et al. Ginsenoside Rb1 protects against diabetes-associated metabolic disorders in Kkay mice by reshaping gut microbiota and fecal metabolic profiles. *J Ethnopharmacol*. 2023;303:115997. https://doi.org/10.1016/j.jep.2022.115997.

19 Demir S, Nawroth PP, Herzig S, et al. Emerging targets in type 2 diabetes and diabetic complications. *Adv Sci (Weinh)*. 2021;8(18):e2100275. https://doi.org/10.1002/advs.202100275.

20 Ma LL, Yuan YY, Zhao M, et al. Mori Cortex extract ameliorates nonalcoholic fatty liver disease (NAFLD) and insulin resistance in high-fat-diet/streptozotocin-induced type 2 diabetes in rats. *Chin J Nat Med*. 2018;16(6):411-417. https://doi.org/10.1016/S1875-5364(18)30074-8.

21 Wojcikowski K, Gobe G. Animal studies on medicinal herbs: predictability, dose conversion and potential value. *Phytother Res*. 2014;28(1):22-27. https://doi.org/10.1002/ptr.4966.

22 Shen W, Chuang CC, Martinez K, et al. Conjugated linoleic acid reduces adiposity and increases markers of browning and inflammation in white adipose tissue of mice. *J Lipid Res*. 2013;54(4):909-922. https://doi.org/10.1194/jlr.M030924.

23 Liao J, Hao C, Huang W, et al. Network pharmacology study reveals energy metabolism and apoptosis pathways-mediated cardioprotective effects of Shenqi Fuzheng. *J Ethnopharmacol*. 2018;227:155-165. https://doi.org/10.1016/j.jep.2018.08.029.

24 Fang S, Dong L, Liu L, et al. HERB: a high-throughput experiment- and reference-guided database of traditional Chinese medicine. *Nucleic Acids Res*. 2021;49(D1):D1197-D1206. https://doi.org/10.1093/nar/gkaa1063.

25 Kong X, Liu C, Zhang Z, et al. BATMAN-TCM 2.0: an enhanced integrative database for known and predicted interactions between traditional Chinese medicine ingredients and target proteins. *Nucleic Acids Res*. 2024;52(D1):D1110-D1120. https://doi.org/10.1093/nar/gkad926.

26 Ngo LP, Owiti NA, Swartz C, et al. Sensitive CometChip assay for screening potentially carcinogenic DNA adducts by trapping DNA repair intermediates. *Nucleic Acids Res*. 2020;48(3):e13. https://doi.org/10.1093/nar/gkz1077.

27 Yan J, Wang C, Jin Y, et al. Catalpol ameliorates hepatic insulin resistance in type 2 diabetes through acting on AMPK/NOX4/PI3K/AKT pathway. *Pharmacol Res*. 2018;130:466-480. https://doi.org/10.1016/j.phrs.2017.12.026.

28 Liu L, Wang ZB, Song Y, et al. Simultaneous determination of eight alkaloids in rat plasma by UHPLC-MS/MS after oral administration of *Coptis deltoidea* C. Y. Cheng et Hsiao and *Coptis chinensis* Franch. *Molecules*. 2016;21(7):913. https://doi.org/10.3390/molecules21070913.

29 Feng X, Wang K, Hu X, et al. Systematic screening and characterization of absorbed constituents and *in vivo* metabolites in rats after oral administration of Rhizoma Coptidis using UPLC-Q-TOF/MS. *Biomed Chromatogr*. 2020;34(10):e4919. https://doi.org/10.1002/bmc.4919.

30 Liu Y, Zhang Y, Meng Q, et al. Metabolic profile of alkaloids in Rhizoma Coptidis in rat plasma, urine and feces after oral administration using ultra-high-performance liquid chromatography coupled with quadrupole time-of-flight mass spectrometry. *Rapid Commun Mass Spectrom*. 2020;34(9):e8763. https://doi.org/10.1002/rcm.8763.

31 Feng X, Wang K, Cao S, et al. Pharmacokinetics of five alkaloids and their metabolites in normal and diabetic rats after oral administration of Rhizoma Coptidis. *Planta Med*. 2022;88(11):921-932. https://doi.org/10.1055/a-1506-1627.

32 Dong WW, Han XZ, Zhao J, et al. Metabolite profiling of ginsenosides in rat plasma, urine and feces by LC-MS/MS and its application to a pharmacokinetic study after oral administration of *Panax ginseng* extract. *Biomed Chromatogr*. 2018;32(3):e4105. https://doi.org/10.1002/bmc.4105.

33 Liu C, Yang T, Zhao Z, et al. Effects of particle size reduction combined with *β*-cyclodextrin on the *in vitro* dissolution and *in vivo* relative bioavailability of ginsenosides in *Panax ginseng*. *Food Funct*. 2022;13(21):10882-10894. https://doi.org/10.1039/D2FO01098D.

34 Chen Q, Xiao S, Li Z, et al. Chemical and metabolic profiling of Si-Ni Decoction analogous formulae by high performance liquid chromatography-mass spectrometry. *Sci Rep*. 2015;5:11638. https://doi.org/10.1038/srep11638.

35 Miao WJ, Hu Y, Jia L, et al. Profiling and identification of chemical components of Shenshao Tablet and its absorbed components in rats by comprehensive HPLC/DAD/ESI-MS^n analysis. *Chin J Nat Med*. 2018;16(10):791-800. https://doi.org/10.1016/S1875-5364(18)30119-5.

36 Perng W, Conway R, Mayer-Davis E, et al. Youth-onset type 2 diabetes: the epidemiology of an awakening epidemic. *Diabetes Care*. 2023;46(3):490-499. https://doi.org/10.2337/dci22-0046.

37 Ma H, He K, Zhu J, et al. The anti-hyperglycemia effects of Rhizoma Coptidis alkaloids: a systematic review of modern pharmacological studies of the traditional herbal medicine. *Fitoterapia*. 2019;134:210-220. https://doi.org/10.1016/j.fitote.2019.03.003.

38 Abdelazim A, Khater S, Ali H, et al. *Panax ginseng* improves glucose metabolism in streptozotocin-induced diabetic rats through 5' adenosine monophosphate kinase up-regulation. *Saudi J Biol Sci*. 2019;26(7):1436-1441. https://doi.org/10.1016/j.sjbs.2018.06.001.

39 Li X, Liu Z, Liao J, et al. Network pharmacology approaches for research of traditional Chinese medicines. *Chin J Nat Med*. 2023;21(5):323-332. https://doi.org/10.1016/S1875-5364(23)60429-7.

40 Li M, Chi X, Wang Y, et al. Trends in insulin resistance: insights into mechanisms and therapeutic strategy. *Signal Transduct Target Ther*. 2022;7(1):216. https://doi.org/10.1038/s41392-022-01073-0.

41 Petersen MC, Vatner DF, Shulman GI. Regulation of hepatic glucose metabolism in health and disease. *Nat Rev Endocrinol*. 2017;13(10):572-587. https://doi.org/10.1038/nrendo.2017.80.

42 Rines AK, Sharabi K, Tavares CDJ, et al. Targeting hepatic glucose metabolism in the treatment of type 2 diabetes. *Nat Rev Drug Discov*. 2016;15(11):786-804. https://doi.org/10.1038/nrd.2016.151.

43 Perry RJ, Samuel VT, Petersen KF, et al. The role of hepatic lipids in hepatic insulin resistance and type 2 diabetes. *Nature*. 2014;510(7503):84-91. https://doi.org/10.1038/nature13478.

44 Martinez B, Ortiz RM. Thyroid hormone regulation and insulin resistance: insights from animals naturally adapted to fasting. *Physiology (Bethesda)*. 2017;32(2):141-151. https://doi.org/10.1152/physiol.00018.2016.

45 Gauthier BR, Sola-García A, Cáliz-Molina M, et al. Thyroid hormones in diabetes, cancer, and aging. *Aging Cell*. 2020;19(11):e13260. https://doi.org/10.1111/acel.13260.

46 He F, Huang Y, Song Z, et al. Mitophagy-mediated adipose inflammation contributes to type 2 diabetes with hepatic insulin resistance. *J Exp Med*. 2021;218(3):e20201416. https://doi.org/10.1084/jem.20201416.

47 Mahboobifard F, Pourgholami MH, Jorjani M, et al. Estrogen as a key regulator of energy homeostasis and metabolic health. *Biomed Pharmacother*. 2022;156:113808. https://doi.org/10.1016/j.biopha.2022.113808.

48 Yan H, Yang W, Zhou F, et al. Estrogen improves insulin sensitivity and suppresses gluconeogenesis *via* the transcription factor Foxo1. *Diabetes*. 2019;68(2):291-304. https://doi.org/10.2337/db18-0638.

49 De Paoli M, Zakharia A, Werstuck GH. The role of estrogen in insulin resistance: a review of clinical and preclinical data. *Am J Pathol*. 2021;191(9):1490-1498. https://doi.org/10.1016/j.ajpath.2021.05.011.

50 Joshi MB, Ahamed R, Hegde M, et al. Glucose induces metabolic reprogramming in neutrophils during type 2 diabetes to form constitutive extracellular traps and decreased responsiveness to lipopolysaccharides. *Biochim Biophys Acta Mol Basis Dis*. 2020;1866(12):165940. https://doi.org/10.1016/j.bbadis.2020.165940.

51 Yang S, Wang S, Chen L, et al. Neutrophil extracellular traps delay diabetic wound healing by inducing endothelial-to-mesenchymal transition *via* the Hippo pathway. *Int J Biol Sci*. 2023;19(1):347-361. https://doi.org/10.7150/ijbs.78046.

52 Lawan A, Bennett AM. Mitogen-activated protein kinase regulation in hepatic metabolism. *Trends Endocrinol Metab*. 2017;28(12):868-878. https://doi.org/10.1016/j.tem.2017.10.007.

53 Steinberg GR, Hardie DG. New insights into activation and function of the AMPK. *Nat Rev Mol Cell Biol*. 2023;24(4):255-272. https://doi.org/10.1038/s41580-022-00547-x.

54 Steneberg P, Lindahl E, Dahl U, et al. PAN-AMPK activator O304 improves glucose homeostasis and microvascular perfusion in mice and type 2 diabetes patients. *JCI Insight*. 2018;3(12):e99114. https://doi.org/10.1172/jci.insight.99114.